Properties of Poly(isoprene): Model Building in the Melt and in Solution

Roland Faller*

Department of Chemical Engineering & Materials Science, University of California−Davis, Davis, California 95616

Dirk Reith†

Max-Planck-Institut für Polymerforschung, 55128 Mainz, Germany

Received November 26, 2002; Revised Manuscript Received May 7, 2003

ABSTRACT: Properties of 1,4-*trans*-poly(isoprene) at ambient conditions are determined by simulations on two length scales based on two different models: a fully atomistic and a mesoscopic one. The models are linked via a mapping scheme such that one mesoscopic bead represents one chemical repeat unit. Melts as well as solutions of several chain lengths are investigated and mapped individually to the meso-scale. The resulting models are compared to each other. The meso-scale models could be simulated over a large variety of chain lengths and time scales relevant for experimental comparison. Concerning static properties, we determine the persistence length and the scaling behavior of the radius of gyration. The latter is compared to experiments, and the agreement is satisfactory. Furthermore, we find deviations from Rouse dynamics at all chain lengths at ambient conditions.

I. Introduction

Poly(isoprene), better known as rubber, is one of the most commonly used polymers. Its natural form, kautschuk, is highly abundant in nature, and for technological purposes, synthetic variations are easily industrially polymerized from isoprene.[1] As an elastomer, its rich field of technical applications comprises tires, textiles, or cable coatings.[2] Still, some of its static as well as dynamic properties are not yet understood on a microscopic basis.

The time and length scales important for the investigation of polymeric materials generally cover a wide range—from angstroms and picoseconds to millimeters and eventually hours. There is no hope to capture all important quantities of a system with one single model. Thus, computational methods have to be developed to use the information in more detailed models as an input for coarser models, allowing to investigate larger systems. The most prominent example is the step from quantum chemistry (based on Schroedinger's equation) to semiempirical atomistic models (based on Newton's equation of motion). For many modern applications this step is not sufficient. So, the mapping of atomistic systems to meso-scale systems (in which monomers, thought of as "super-atoms", are the smallest units of the simulation) became the focus of several studies.

Coarse-graining (CG) approaches have reached considerable attention over the past decades; for a recent review see ref 3. The basic idea of all CG schemes is to separate the system into fast and slow variables where the fast degrees of freedom are not of primary interest for the question under study. Thus, a model can be compiled containing the slow degrees of freedom only. Recently methods have become available to perform coarse graining in a polymer-specific and systematic way.[4−7] We refer to a systematic procedure if the identity of the polymer is not lost during the mapping procedure. Moreover, the purpose of such techniques is to develop meso-scale models for the simulation of large systems of specific polymers. To ease the mapping procedure, two automatic optimization schemes have been developed by our co-workers and us: a simplex algorithm technique[5,8] and the iterative Boltzmann inversion method which directly targets the problem of structure differences with a physically motivated approach.[7] Similar ideas have been applied to reproduce experimental data in atomistic simulations.[9]

The goal here is that two models on different length scales should produce the same distribution functions on the larger of the two length scales. Then, we can regard them representing the same polymer. Because of its rich applications, we take poly(isoprene) as an example. Additionally, we point out some differences to recent findings in studies of semigeneric bead−spring models incorporating stiffness as the only local characteristics.[10,11]

II. Investigations with Atomistic Detail

As a basis for our mapping procedure we need atomistic simulations with good accuracy. We performed simulations with appropriately designed force fields reproducing the atomistic structure and thermodynamics very reliably.

A. Melt Investigations. The atomistic melt simulations have been described in detail in ref 12. Let us briefly summarize the main characteristics. The simulation box contains 100 oligomers of average length 10 monomers. All chains represent *trans*-poly(isoprene) (cf. Figure 1). We use a self-developed all-atom force field resulting in 132 interaction sites for a 10-mer;[12] every atom is represented by one interaction site (cf. Tables 1−3). The simulations lasted for 1−2 ns at ambient conditions ($T = 300$ K, $p = 101.3$ kPa); cf. Table 4. The model is capable of describing local reorientation func-

† Present address: DaimlerChrysler AG, HPC G202, Fronaeckerstr. 40, D-71059 Sindelfingen, Germany.

* To whom correspondence should be addressed. E-mail: rfaller@ucdavis.edu.

10.1021/ma025877s CCC: $25.00
Published on Web 06/10/2003

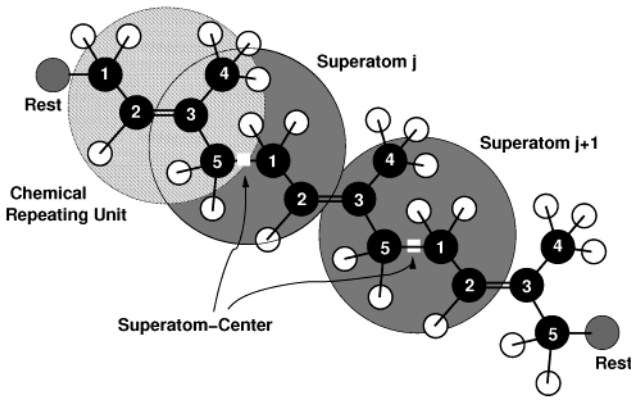

Figure 1. Illustration of the mapping of *trans*-1,4-poly(isoprene) from the atomistic to the mesoscopic level. Each chemical repeat unit is represented by one super-atom. As center of these super-atoms, we choose the middle of the atomistic bond between two successive chemical repeat units (marked by a outlined square). This is useful because the resulting mapped chains generate well-distinguishable peaks for the various intramolecular distributions.

Table 1. Angles (Equilibrium Values ϕ_0 and Potential Strength k) and Bond Lengths[a] l_b for Atomistic Melt Simulations of Poly(isoprene)

angle	ϕ_0 [deg]	k[kJ/(mol rad^2)]	bond	l_b [nm]
$C_1-C_2-C_3$	128.7	250	C_1-C_2	0.150
$C_2-C_3-C_4$	124.4	250	$C_2=C_3$	0.1338
$C_2-C_3-C_5$	120.2	250	C_3-C_4	0.151
$C_4-C_3-C_5$	115.4	250	C_3-C_5	0.1515
$C_3-C_5-C_1$	114.5	250	C_5-C_1	0.155
$C_5-C_1-C_2$	112.7	250	C−H	0.109
$C-C_{sp3}-H$	109.5	250		
C_1-C_2-H	114.4	250		
C_3-C_2-H	114.4	250		
H−C−H	109.5	250		

[a] The bond lengths are constrained using SHAKE.[33]

Table 2. Force-Field Parameters of the Nonbonded Interactions for Atomistic Melt Simulations of Poly(isoprene)[a]

atom	m [amu]	σ [nm]	ϵ [kJ/mol]
C_{sp2}	12.01	0.321	0.313
C_{sp3}	12.01	0.311	0.313
H	1.00782	0.24	0.2189

[a] m is the atom mass, σ the interaction radius, and ϵ the interaction strength.

Table 3. Force-Field Parameters of the Dihedral Angles for Atomistic Melt Simulations of Poly(isoprene)[a]

torsion	equilib angle τ_0 [deg]	barrier k_τ [kJ/mol]	periodicity i
1	0	5.2	1
1	0	−7.4	2
1	0	10.0	3
2	180	9.7	1
2	180	14.1	3
3	0	−21.1	1
3	0	−12.3	2
3	0	0.5	3

[a] Torsions 1 to 3 are numbered from left to right (cf. Figure 1). Torsion 1 corresponds to the bond between atoms 3 and 5.

tions in comparison to NMR measurements and reproduces reasonably the melt structure factor of poly(isoprene).[12,13]

Nonbonded interactions between atoms connected by any bonding potential and the so-called "1−5" and "1−6" interactions were excluded. Constant temperature and pressure are ensured using Berendsen's method[14] with time constants 0.2 ps for temperature and 8 ps for pressure. The pressure coupling using a compressibility of 2×10^{-7} kPa^{-1} was employed for the three Cartesian directions independently. All simulations were performed using the YASP molecular simulation package[15] with a time step of 1 fs and a cutoff for the nonbonded interactions at 0.9 nm. Configurations were saved every picosecond. No charges were used through the simulations.

Table 4. Summary of the Characteristics of the Atomistic Melt Simulations

system	T [K]	t_{sim} [ps]	M_w/M_n	ρ [kg/m^3]
M1	300	1184	1.00	890
M2	300	2012	1.05	917.4
M3	300	1737	1.05	916.8
M3	413	792	1.05	826

B. Atomistic Simulations of Poly(isoprene) in Solution of Cyclohexane. For the atomistic simulations of *trans*-PI in cyclohexane we used the same force field as in the melt simulations, except that only interactions up to 1−4 interactions (inclusive) are excluded. Again we restrict ourselves to a brief summary as the simulations of the solution are described in detail in ref 16. The cyclohexane force field was developed using the automatic simplex method[9] and tested in the dynamics of mixtures of cyclohexene and cyclohexane.[17] For this study we augmented the cyclohexane force field with torsion potentials along the ring in order to avoid inadvertent flipping between the chair and boat configuration. The original cyclohexane force field and its torsion revision are found in refs 9 and 16. The densities of the solutions increase slightly with concentration of polymer (Table 5). They are very close to the density of pure cyclohexane without torsions (767.7 kg/m^3),[9,17] which in turn was optimized against experimental data. We did not reoptimize the Lennard-Jones parameters. Therefore, the pure cyclohexane system has a slightly lower density as the molecules are less flexible and less spherical due to the torsions. To decide on the quality of the solvent the radius of gyration

$$R_G = \sqrt{\sum_i (m_i r_i^2)/\sum_i m_i}, \quad \vec{r}_i = \vec{R}_i - \langle \vec{R}_i \rangle \qquad (1)$$

and the end-to-end length are important characteristics. The mean-square end-to-end distance $\sqrt{\langle R_{e-e}^2 \rangle}$ is measured between the terminal carbons of the chain. Additionally, the hydrodynamic radius R_H was calculated as the first inverse moment of the distance vectors:[18]

$$\frac{1}{R_H} = \frac{1}{N^2}\left\langle \sum_{i \neq j} \frac{1}{r_{ij}} \right\rangle \qquad (2)$$

Here, N represents the number of monomers of the chain and r_{ij} the distance between two arbitrarily chosen super-atoms i and j.

We do not find a systematic variation of the radius of gyration with concentration. In the system with two chains in a solvent of 500 molecules the two chains behave differently whereas in the more highly concentrated systems the radii of gyration are very close although they were also started with the same initial configurations as the other two chain system. The

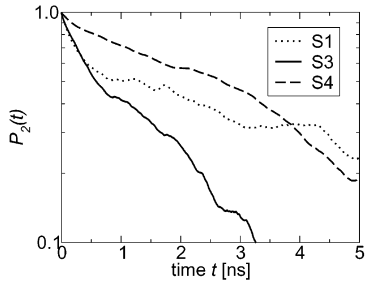

Figure 2. Reorientation correlation function of whole chains in solution in semilogarithmic representation. We show the second Legendre polynomial P_2 of the reorientation angle. The shortcuts S1, S3, and S4 are defined in Table 5.

autocorrelation functions of the gyration radii decays on the scale of less than 100 ps. The systems are equilibrated; still the error bars are quite large. To decrease them substantially, much larger simulations would be necessary. This was not the purpose of the atomistic simulations as the long time scales are left to the coarse-grained model to be developed here.

In Figure 2 we show the decay of the reorientation correlation function of the end-to-end vector of the whole chains in solution. This function overall follows an exponential tendency, and the correlation time is on the order of 2−4 ns, showing reasonable equilibration. Additionally, the overall reorientation becomes slower with increasing concentration. The dynamics of the solvent is found to slow down and become more anisotropic with increasing concentration.[16]

Atomistic molecular dynamics cannot equilibrate such a system to the absolute decay of the end-to-end correlation function even for a oligomer system. This again shows the necessity to deal with even relatively simple solutions of oligomers in a multiscale way. Nonetheless, as we are able to decrease the correlation function of the overall reorientation to below 30% for the slowest system, we have a good starting point for our multiscale approach, especially as we combine the different independent systems.

III. The Mapping Procedure

The mapping procedure is the same for both the melt and the solution system. It has been described in full detail in ref 7, so we limit ourselves to a short summary. Distribution functions from atomistic simulations are the basis of the mapping, since the mesoscale model is optimized against them. In this study, M1 (for the melt) and the combination of S1 and S3 (for the solution) were chosen as parent atomistic simulations (see Tables 4 and 5). The mapping itself is illustrated in Figure 1. Each chemical repeat unit is replaced by one super-atom (interaction center), located in the middle of the atomistic bond between successive chemical repeat units. Consequently, an atomistic N-mer will be coarse-grained to a $(N - 1)$-mer. The reasoning behind this choice is that the such mapped super-atoms are more spherical compared to the case in which one would have chosen the center of mass of the real monomer. The advantage is that the mapped chains generate well-distinguishable peaks for the various intramolecular distributions. For long chains the error introduced due to the missing rests is negligible.

In this contribution, we use exclusively the pressure-corrected CG force field which has been optimized by the inverted Boltzmann method.[7] The inverted Boltzmann method utilizes the differences in the potentials of mean force between the distribution functions generated from a trial potential and the true distribution functions to improve the effective potential successively. We would like to derive an effective nonbonded potential $V_\infty(r)$ from a given tabulated start potential $V_0(r)$, targeting to match the radial distribution function $g_\infty(r)$. Simulating our system with $V_0(r)$ will yield a corresponding $g_0(r)$ which is different from $g_\infty(r)$. The potential therefore needs to be improved, which is done by a correction term $-k_BT \ln[(g_0(r)/g(r)]$. This step can be iterated as follows by

$$V_{j+1}(r) = V_j(r) - k_BT \ln\left(\frac{g_j(r)}{g(r)}\right) \tag{3}$$

until

$$f_{\text{target}} = \int_{r_{\min}}^{r_{\max}} \omega(r)(g_\infty(r) - g_j(r))^2 \, dr \tag{4}$$

falls below an initially specified threshold. We apply $w(r) = \exp(-r)$ as weighting function in order to specifically penalize deviations at small distances. Note that all potentials derived this way are known purely numerically. We do not attempt to use analytic functions.

Pressure corrections can be introduced in polymer systems by adding a weak linear potential term to the attractive long-range part of $V_j(r)$ as in most cases the initially optimized structure corresponds to a pressure different from the one at which the atomistic simulations are performed. We then postoptimize the structure of the system according to the above scheme in turn with linear additions until also the pressure matches the atomistic system. The pressure correction is of the form

$$V_{\text{linpc}} = A\left(1 - \frac{r}{r_{\text{cutoff}}}\right), \quad A = -0.1kT \tag{5}$$

Taking this as a starting condition, we reoptimize the system against the structure. This combined method was iterated until the structure and the pressure were in agreement with target values. The pressure correction mainly acts on the longer-range attraction whereas the structure is dominated by the short-range repulsion.

We do not only optimize the nonbonded interactions but additionally the intrachain bonded interactions. The bonds between super-atoms were taken as harmonic bonds to reproduce the distance found in the atomistic simulations. The way we chose the interaction center for the super-atoms allowed us to use a simple harmonic potential. It has been shown[10,19] that local stiffness can play a crucial role in the local dynamics. To model such a stiffness more realistically, also bond angle distributions on the super-atom level have been recorded in the atomistic simulations. These distributions are used then as target functions in exactly the same way the radial distribution functions are used for the nonbonded interactions. This allows us not only to use the persistence length as a local characteristics but also to include a more detailed description of the intrachain interactions. These "super-bond angles" connecting three super-atoms depend on six consecutive atomistic torsion potentials, so that the local conformations enter in the coarse-grained model in a systematic way. For simplicity, we did not include torsion potentials on the coarse-grained level. The recorded distributions were flat enough in order to neglect them.[7]

Table 5. Thermodynamic and Static Properties of the Solution[a]

system	N_P	N_C	c [%]	ρ [kg/m^3]	t_{sim} [ns]	R_H [nm]	R_G [nm]	R_e^2/R_G^2
S0	0	500	0.0	756.3	1.0			
S1	1	250	4.6	764.2	11.25	1.33 ± 0.12	1.21 ± 0.20	6.1
S2	1	500	2.4	757.5	5.58	1.40 ± 0.05	1.26 ± 0.10	6.0
S3	2	500	4.6	762.5	7.81	1.34 ± 0.10	1.23 ± 0.20	6.5
S4	2	250	8.9	768.2	11.56	1.37 ± 0.09	1.29 ± 0.15	7.2

[a] Details of the different systems and the numbers with which they are referenced in the following. N_P is the number of oligomers ($C_{75}H_{122}$) and N_C the number of cyclohexane molecules. c is the concentration in weight % polymer. t_{sim} is the simulated time for the systems.

Table 6. Data of the Mesoscopic Brownian Dynamics Poly(isoprene) Melt Simulations[a]

chain length N	9	15	20	35	40	45	50	65	85	100	120
no. of chains N_c	100	150	150	100	150	150	80	130	50	120	100
pressure p^*	±0.0	−0.01	−0.04	−0.15	−0.07	−0.08	−0.08	−0.08	−0.09	−0.09	−0.09
simulation time [10^6 time steps]	3.0	4.0	4.0	7.2	6.0	6.0	8.0	6.0	8.0	6.0	6.0
R_G [nm]	0.75	1.03	1.20	1.63	1.75	1.87	1.97	2.25	2.63	2.85	3.14
R_H [nm]	1.11	1.19	1.27	1.50	1.60	1.65	1.69	1.98	1.98	2.21	2.42
R_G/R_H	0.68	0.86	0.94	1.09	1.10	1.13	1.17	1.14	1.33	1.29	1.30
R_e^2/R_G^2	6.0	6.0	6.0	6.0	6.0	6.0	6.0	6.0	6.0	6.0	6.0
D_{center} [10^{-6} cm^2/s]	16.6	10.7	6.7	4.2	2.5	2.3	2.9	1.3	1.3	0.8	0.6
D_{com} [10^{-6} cm^2/s]	16.0	10.9	6.7	4.1	2.5	2.3	2.8	1.3	1.2	0.8	0.6

[a] The pressure is stated in reduced units.[20] All systems are simulated at a temperature of $T = 300$ K and at a density of $\rho_p = 7.25$ monomers/nm^3 and correspond to the atomistic simulation M1. The static properties come with a standard error of ≈5% and the dynamic properties with an error of ≈15%. For the dynamic mapping at this temperature we used the method described in ref 34.

Further details of the optimization procedure of different systems, including the two systems discussed here, can be found in ref 7. For the polymer melt system three iterations were enough to reproduce a radial distribution function which was virtually indistinguishable from the target except for the pressure correction. It took 10 cycles to get a sufficient accuracy in both structure and pressure.

IV. Mesoscale Simulations

A. Technical Simulation Details. Brownian dynamics (BD, for the melt) and Monte Carlo (MC, for the solution) simulations have been performed on the mesoscale level. All BD runs used the *NVT* ensemble, with values for density and temperature corresponding to the values of the parent atomistic simulation. The systems consisted of an orthorhombic box employing periodic boundary conditions. Langevin equations of motion were integrated by the velocity Verlet algorithm with a time step $\Delta t = 0.01\tau$[20] at a dimensionless temperature of $T^* = 1$. This temperature was maintained by the Langevin thermostat with friction constant $\Gamma = 0.5\tau^{-1}$.[21] For the MC simulations representing the solution case, a single chain program was used.[22] The code uses various kinds of Pivot moves to get the equilibrium distribution of a single chain in the canonical ensemble. Here, 10^5 accepted equilibration moves were carried out before a production run of 10^6 accepted moves was started. For analysis, every 500th configuration was stored, in both BD and MC simulations.

B. Static Properties in the Melt and in Solution. The results of the CG simulations are summarized in Table 6 for the poly(isoprene) melts and in Table 7 for the solutions. In both cases the radius of gyration R_G and the hydrodynamic radius R_H are correctly reproduced compared to the values of the parent atomistic simulations (within standard errors).

Extensive Brownian dynamics simulations were carried out to investigate the static and the dynamic behavior of poly(isoprene) melts. The coincidence (within statistical fluctuations) of the values for D_{center} and D_{com}, representing the diffusion coefficient of the central monomer of the chain and their center of mass, shows that the system is truly equilibrated. Let us first concentrate on the static properties. In Table 6 we list the values for the radius of gyration R_G, the hydrodynamic radius R_H, their ratio, and the ratio R_e^2/R_G^2 which provide information about the extension of the chains. The scaling behavior of R_G is shown in Figure 3. A fit for $N \geq 35$ yields a scaling exponent of $\nu = 0.53$, which is slightly larger than the ideal value for melts of $\nu_{melt} = 0.5$, suggesting that the chains are not sufficiently close to the limit of infinitely long chains. This is also supported by the ratio R_G/R_H, which is well below the infinite limit of around 1.5. The fact that $R_e^2/R_G^2 =$

Table 7. Static Properties (with Standard Errors of ≈5%) As Obtained from Monte Carlo Simulations of Mesoscopic Poly(isoprene) Solutions[a]

chain length N	9	15	35	50	85	100	120
R_G [nm]	0.91	1.33	2.37	2.92	4.11	4.48	4.98
R_H [nm]	1.23	1.40	1.98	2.32	3.06	3.31	3.63
R_G/R_H	0.74	0.95	1.20	1.26	1.34	1.35	1.37
R_e^2/R_G^2	7.3	7.1	6.7	6.5	6.5	6.4	6.4

[a] The system density and temperature correspond to the parent atomistic systems S1 and S3.

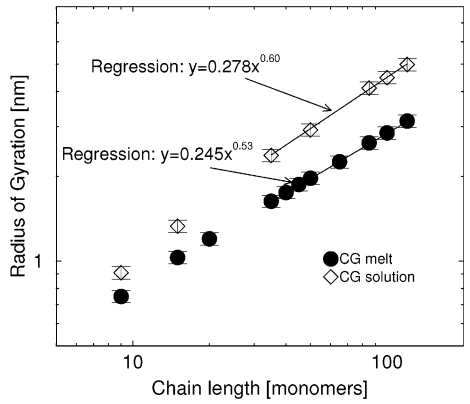

Figure 3. Scaling behavior of CG poly(isoprene) chains in melt (filled circles) and solution (open diamonds).

6.0 holds for all chain lengths shows that the static behavior corresponds to random walks.

Table 7 shows the results of the poly(isoprene) solution systems. Since we applied MC, static properties are listed exclusively. The scaling behavior of R_G is also presented in Figure 3. With a fit for the same region as in the melt case ($N \geq 35$) we obtain a scaling exponent of $\nu = 0.60$. This is slightly larger than the theoretical value $\nu_{gs} = 0.588$ for polymers in good solvents due to the finite chain length. The ratio R_e^2/R_G^2 decreases monotonically with chain length. This indicates that the intramolecular interactions of poly(isoprene) in the trans state locally stretch the chains.

To the best of our knowledge, only chain size measurements of *cis*-poly(isoprene) in solution of cyclohexane have been performed.[23,24] Our data coincide within the order of magnitude with the extrapolated experimental data of Tsunashima et al. to our longest chains. Applying their relation for the gyration radius, we calculate 2.76 nm for a chain length of 100 monomers in Θ-solution. This is almost exactly our value for the chains of this length in the melt where also random walk statistics is supposed to apply. Davidson et al. measured the radius of gyration of a mixture of *cis*- and *trans*-poly(isoprene) under good solvent conditions by various techniques including wide-angle light scattering for molecular weight range of 112 000 g/mol and higher.[23] This corresponds to chain lengths of 1650 monomers and longer. Extrapolating the simulation data to the two shortest chains experimentally available, we get 23.7 nm for 112 000 g/mol compared to 17.7 nm experimentally and 26.5 nm for 164 000 g/mol against 19.4 nm experimentally. Thus, we overestimate the gyration radii by about 35%. However, one has to keep in mind that the experimentally investigated system contains a mixture of the trans and cis conformers. The experimentally observed scaling exponent is 0.545 and therefore lower than our exponent of 0.6 and the theoretically predicted exponent of 0.588.

Next, the persistence length l_p of poly(isoprene) was estimated by the decay of the orientation correlation along the chain backbone. The point where this correlation arrives at $y = \exp(-1)$ is a good approximation of l_p

$$\langle \vec{u}_k(n+j)\, \vec{u}_k(n) \rangle = \exp\left(-\frac{j l_b}{l_p}\right) \tag{6}$$

Here, l_b is the bond length and $\vec{u}_k(n)$ represents the unit vector along the chain, centered at monomer n and pointing to monomer k. The result is shown in Figure 4. The bonds are completely decorrelated beyond the fourth neighbor for the melt. For the persistence length, $l_p \approx 1.25 l_b$ (= 0.59 nm) can be estimated. As expected, this is independent of chain length; all curves fall on top of each other. The same holds for the solution case. Here the persistence length could be estimated to be $l_p \approx 2.7 l_b$ (= 1.27 nm), i.e., more than twice as large as in the melt. So, the concentration of poly(isoprene) chains has a strong influence on the intrachain statistics. The dense packing in the melt favors a quick decorrelation between neighboring chain monomers.

Finally, we can compare some of the above results to data for a melt of generic bead−spring chains with bond-angle stiffness.[13,19] It has already been used to successfully map the dynamic behavior of atomistic poly-

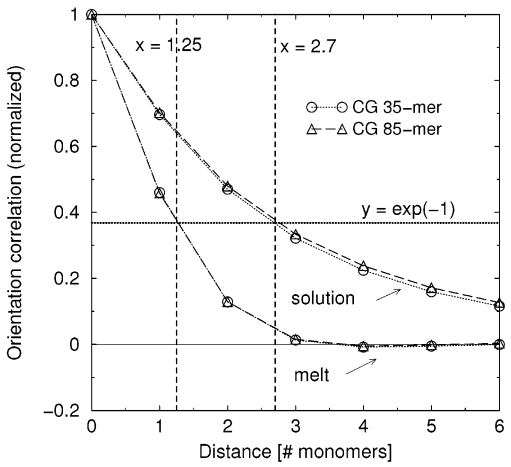

Figure 4. Approximation of the persistence length l_p of some arbitrarily picked CG poly(isoprene) systems. Using eq 6, the decay of the orientation correlation function to $y = \exp(-1)$ approximates l_p. In the melt this yields $l_p \approx 1.25 l_b$, and for the solution $l_p \approx 2.7 l_b$. Errors are on the order of the symbol sizes.

Table 8. Results of Some Static Properties for a Realistic Meso-Scale Model of Poly(isoprene) in a Melt and a More Generic Bead−Spring Model with Bond Angle Stiffness[a]

melt model	R_G [nm]	R_e^2 [nm^2]	R_e^2/R_G^2	l_p [monomers]	l_K [nm]
$x = 1.5$, $N = 20$[13]	1.28	10.3	6.3	1.2	1.2
CG PI, $N = 20$	1.20	8.7	6.0	1.25	1.0
$x = 1.5$, $N = 50$[13]	2.20	29.5	6.2	1.3	1.3
CG PI, $N = 50$	1.97	23.3	6.0	1.25	1.0

[a] R_G is the radius of gyration, R_e is the end-to-end distance of the chain, l_p corresponds to the persistence length, and l_K corresponds to the Kuhn segment length.

(isoprene) to the meso-scale,[11] even though it just comprised one simple bond angle potential in addition to a FENE bead−spring interaction for the intramolecular part:

$$V_{angle} = x[1 + \vec{u}_j \cdot \vec{u}_{j+1}] k_B T \tag{7}$$

The vector $\vec{u}$ corresponds to a normalized bond vector, and x is the force constant to determine the stiffness. The scalar product corresponds to the cosine of the angle along the backbone. The comparison of static properties of the two models is presented in Table 8. One observes that most properties yield similar values, in the case of R_G, R_e^2/R_G^2, and l_p even within statistical error. However, the end-to-end distances deviate more strongly, showing that the realistic poly(isoprene) chains are more coiled than generic chains. This is also reflected in the Kuhn segment length l_K, which defines the distance beyond which one expects universal chain behavior:

$$l_K = \frac{\langle \vec{R}_e^{\,2} \rangle}{R_e^{(max)}} = \frac{\langle \vec{R}_e^{\,2} \rangle}{(N-1) l_b} = C_\infty l_b \tag{8}$$

It is significantly shorter for the realistic model compared to the generic one. A reason for that could be the missing torsional potential in the latter. Also, the dynamical behavior turns out to differ significantly, as will be shown in the next section.

Although the mesoscopic model is optimized against the atomistic structure, some structural differences remain. Comparing the pair distribution functions of

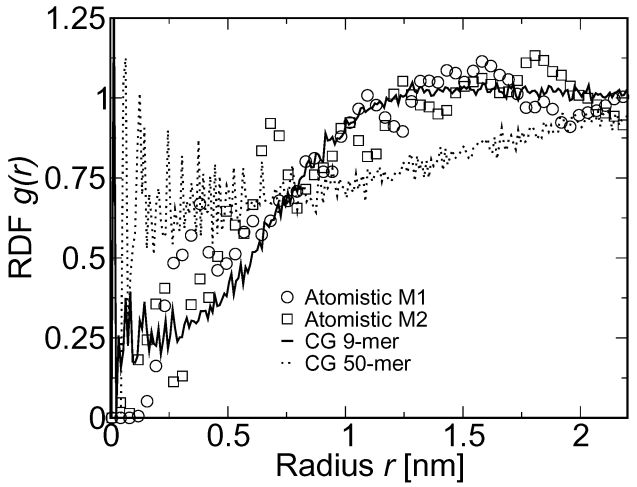

Figure 5. Pair distribution function $g(r)$ for the centers of mass of different chain models. We show two different atomistic 10-mers (M1 and M2), a mesoscopic 9-mer, and a mesoscopic 50-mer. The statistics is weak close to overlap. At distances of 1 nm and more, the errors are about 5%.

centers-of-mass of whole chains (cf. Figure 5), we see that the mesoscopic model chains show less structure on short distances. The mesoscopic 9-mers show a simple correlation hole whereas the atomistic 10-mers exhibit a structured correlation hole. Moreover, we see the strong difference between a mesoscopic 9-mer and a 50-mer. In the latter case the correlation hole is much less pronounced. This can be understood as the bigger a chain becomes, the less volume in its ellipsoid of gyration it actually occupies and the more overlap of such ellipsoids is possible.

C. Dynamical Properties in the Melt. The Rouse model[25] is widely accepted for the dynamics of short flexible chains in the melt. It is based on the screening of excluded volume and that all local intrachain interactions can be mapped onto a Kuhn segment length.[26] Poly(isoprene) has been experimentally tested against the Rouse model,[27] and the agreement was not too good at room temperature. Simulations at the atomistic model found for the oligomers of length 10 a reasonable description by the Rouse model only at the elevated temperature of $T = 413$ K.[11]

For long chains deviations from the Rouse model are expected due to mutual topological constraining of chains. Such deviations could then be attributed to entanglements. Recently, it has been shown that even a weak presence of stiffness can dramatically decrease the onset of entanglement influences.[10] In the present contribution we are using a different and systematic way to derive the intrachain interactions. It is therefore of interest to compare the effect of these more realistic local interactions on the meso-scale level to the Rouse model. We do not attempt to directly map the atomistic and meso-scale dynamics onto each other. However, we use the numerical interaction potentials in a Brownian dynamics simulation and elucidate the influence they exert on the overall dynamics in the melt.

Two observables are commonly used to decide on the validity of the Rouse model: the mean-squared displacements and the Rouse modes. Figure 6 shows the g_1 function which is defined as

$$g_1(t) = \langle(\vec{R}_{\text{center}}(t+t_0) - \vec{R}_{\text{center}}(t_0))^2\rangle_{t_0} \qquad (9)$$

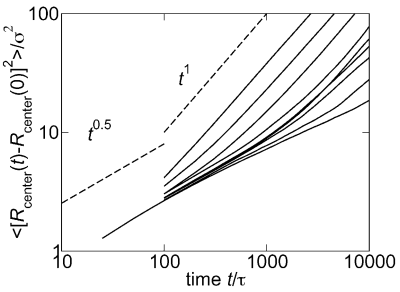

Figure 6. The g_1-function, mean-squared displacement of central monomers for the melt simulation at chain lengths $N = 9$, 15, 20, 35, 40, 45, 50, 85, and 120 from top to bottom. As guides to the eye, we show lines indicating $t^{0.5}$ and t^1. Time and space are rescaled by the usual Lennard-Jones units σ and τ.

where $\vec{R}_{\text{center}}(t)$ denotes the position of the central monomer of a chain at a given time. The central monomer is chosen to suppress end effects as good as possible. For short times ($t < \tau_R$) one expects all curves to fall on top of each other; τ_R is the Rouse time with all internal degrees of freedom are relaxed (below). At such short times the individual monomer does not yet have to drag the whole chain with it, but an increasing part. At $t \approx \tau_R(N)$ the different curves leave the master curve as the increasing neighborhood has reached the chain length. For longer chains Figure 6 shows clearly such a Rouse regime where $g_1(t) \propto t^{0.5}$. Additionally, for all chain lengths $N \leq 85$ we find the free diffusion limit $g_1(t) \propto t$ reached and therefore the systems equilibrated. This shows that the local dynamics is Rouse-like with the connectivity leading to a time-dependent diffusion coefficient for $t < \tau_R$. This in turn leads to the subdiffusive behavior observed. For longer chains the local regime lasts longer which clearly hints toward the connectivity as reason for the subdiffusivity. For the largest chain length of $N = 120$, which corresponds to a molecular weight of 8162 g/mol, we find a small time window (between about 3000τ and 5000τ) where the logarithmic slope falls slightly below 0.5 (namely 0.45). This hints to the first onsets of entanglement influences. As the experimental entanglement length of poly(isoprene) is 6400 g/mol,[28] this shows that approaching it we find a first indication of slowdown which may be attributed to entanglements. It is known that in order to find strong deviations from the $x^{0.5}$ behavior or even approach the $x^{0.25}$ behavior expected from Rouse modes constrained in a reptation tube[18] chain lengths of an order of magnitude longer than the entanglement length are needed.[10,29,30]

The actual Rouse model relies on the independence of the Fourier modes of the chains. We compare the decay of these Rouse modes $\vec{X}_p$

$$\vec{X}_p = \frac{1}{N}\sum_{i=0}^{N-1} \cos\left(\frac{\pi p\left(i+\frac{1}{2}\right)}{N}\vec{R}_i\right) \qquad (10)$$

According to theory, the curves for the different modes at a given chain length should collapse if the time and the correlation function are rescaled by the squared mode index.[18] For intermediate chain lengths we find this scaling to work reasonably well. For longer chain lengths, however, the higher modes are apparently faster than predicted by the Rouse model. This is a first hint toward entanglements. It has been observed in

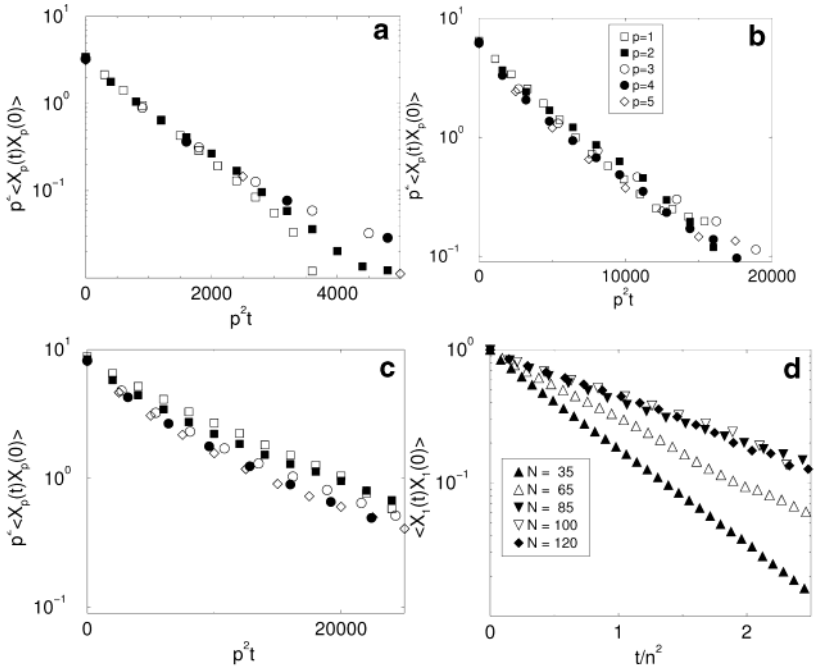

Figure 7. Decay of the autocorrelation functions of the Rouse modes for different chain lengths in Rouse scaling. (a) $N = 35$, (b) $N = 65$, and (c) $N = 85$. The symbols are described in (b). (d) Comparison of the decay of the autocorrelation function for different chain lengths.

Table 9. Fits of the Rouse Time Using the Decay of the first Rouse Mode for Different Chain Lengths[a]

N	τ_R	τ_R/N^2	ζ/kT
35	743	0.60	17.76
50	1946	0.78	23.09
65	3722	0.88	26.04
85	9300	1.29	38.18
100	13800	1.38	40.85
120	17700	1.23	36.41

[a] The estimates have an error of 15%. Also, the Rouse friction coefficient ζ is shown with the same error estimate in units of temperature.

simulations of other polymer models that especially the lower modes are likely to be the first to be influenced by entanglements.[11,31] So for longer chains we get a 2-fold deviation from the Rouse model at high and low modes as the Rouse scaling is no more obeyed.

Table 9 shows the Rouse time τ_R derived by an exponential fit to the first Rouse mode X_1 in dimensionless units. We clearly see finite chain length effects. For longer chains $N \geq 100$ these effects start to become weaker. Figure 7 compares the scaling for several chain lengths. This suggests that poly(isoprene) melts at room temperature do not completely behave according to Rouse theory. From the Rouse times we can calculate a friction coefficient ζ at every chain length which is defined by

$$\zeta = \frac{3p2\pi^2 k_B T \tau_p}{N^2 {l_b}^2} \tag{11}$$

This friction increases with chain length until it reaches a plateau value at $N \geq 80$. This indicates that the Rouse model in this system is only obeyed for the larger chain lengths. The different Rouse modes at a given chain length obey Rouse scaling even for shorter chains, but the Rouse friction assumes only a generic value for chains of intermediate length.

We are not yet able to reach into the entangled regime; we are just reaching at the entanglement length. Especially for the longest chains the scaling of the Rouse modes for different chain lengths onto each other apparently holds. It is interesting to note that we see finite chain length effects for chains of moderate length. Figure 7d is a way to tell oligomers from polymers as the self-similarity is obeyed in the polymer case. For oligomers the Rouse friction calculated from the first Rouse mode increases with chain length (see Table 9). This was not found in a recent study of model chains only incorporating stiffness. In that case the Rouse model was obeyed almost from the very beginning ($N > 15$). This is another important finding in the view of modeling long oligomers or short polymers. For chains with chemical identity we find a regime where the chain nature is already important, but the generic polymer models are not yet valid. These results confirm our earlier results where a very simple three-body interaction was used to vary the local stiffness.[11] In both cases it is clear that intrachain potentials have a marked influence on the overall dynamics of a polymer melt. Moreover, we find that the diffusion coefficient does not scale in a Rouse like manner with chain length. According to Rouse theory, the product of chain length with the diffusion constant DN should be constant, and deviations from such a plateau at high molecular weight can be attributed to entanglements. We see a decrease of DN with chain lengths already at very low molecular weight (cf. Figure 8a). However, this cannot be described by the entanglement effects as all the other indicators hint toward a nonentangled motion. Moreover, in the region where we find Rouse scaling to be fulfilled, namely at $N \geq 80$, the dependence of the diffusion coefficient on molecular weight becomes weaker. Also, if we rescale the quantity DN by multiplication with the friction coefficient, we do not get a constant (cf. Figure 8b). If we would have a perfect random walk with vanishing correlation length and ideal Rouse behavior, we would find $DN\zeta = k_B T$. The values in units of $k_B T$

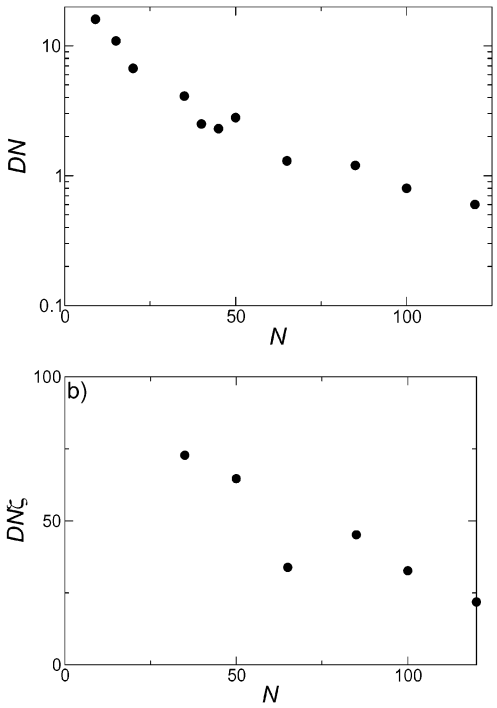

Figure 8. (a) Nondimensionalized center-of-mass diffusion coefficient scaled with chain length. According to Rouse theory, this should be a constant. (b) Nondimensionalized center-of-mass diffusion coefficient rescaled with chain length and chain length dependent friction coefficient (cf. Table 9). The error for both figures is around 15%.

are much larger than unity as the correlation length of the random walk is not 0; note that we did not introduce a persistence or Kuhn length in the analysis. Moreover, also this quantity decays with increasing chain length. This again confirms that the Rouse model cannot fully explain the observations. A possible reason may be the different distances of the temperature from the chain length dependent glass transition temperature T_g. Experiments on polyethylene showed such an effect.[32] Therefore, a determination of glass transition temperatures and simulations at constant temperature distance from T_g may be a way to find correct Rouse scaling in such a system.

V. Conclusions

Atomistic simulations of *trans*-poly(isoprene) in the melt and in solution have been performed and independently coarse-grained to models with one interaction center per monomer. The local scale models are verified against experimental data where available. In the melt a slowdown of the dynamics is found as expected. For the solution we were able to equilibrate oligomers of length 15 monomers until the end-to-end reorientation correlation function decayed to less than about 30% of its initial value. Note that we did not need heavy hardware resources to generate the statistical precision we present here.

The two independently coarse-grained models for solution and melt are distinctly different. It is impossible to represent a chain in such strongly different environments on the coarse-grained level with a generic potential. This is especially true as we aimed to get rid of the solvent completely in the solution case. Melt and solution are very well-known to behave strongly different in the long chain limit.

The coarse-grained models could be compared against well-known long polymer scaling theory. Additionally, comparison to experiments yielded a difference of 35%. The Rouse behavior is for this model recovered for chains of more than around 80 monomers. In summary, we find that the proposed coarse-graining procedure allows us to produce models which are reliably reproducing properties of real polymers. We were not yet able to reach into the reptation regime. Our largest chain length is only slightly above the entanglement molecular weight, and we see a very weak slowing deviation from the Rouse model.

Acknowledgment. Many fruitful discussions with Florian Müller-Plathe and Hendrik Meyer are gratefully acknowledged. Financial support has been provided to R.F. by the Emmy-Noether program of the DFG (German Research Foundation) and to D.R. by the BMBF (German Department of Research) Competence Center in Materials Simulation.

References and Notes

(1) Stevens, M. P. *Polymer Chemistry: An Introduction*; Oxford University Press: Oxford, 1999.
(2) Cowie, J. M. G. *Chemie und Physik der synthetischen Polymere*; Vieweg: Braunschweig, 1997.
(3) Baschnagel, J.; Binder, K.; Doruker, P.; Gusev, A. A.; Hahn, O.; Kremer, K.; Mattice, W. L.; Müller-Plathe, F.; Murat, M.; Paul, W.; Santos, S.; Suter, U. W.; Tries, V. *Adv. Polym. Sci.* **2000**, *152*, 41−156.
(4) Tschöp, W.; Kremer, K.; Batoulis, J.; Bürger, T.; Hahn, O. *Acta Polym.* **1998**, *49*, 61−74.
(5) Reith, D.; Meyer, H.; Müller-Plathe, F. *Macromolecules* **2001**, *34*, 2335−2345.
(6) Akkermanns, R. L. C.; Briels, W. J. *J. Chem. Phys.* **2001**, *114*, 1020−1031.
(7) Reith, D.; Pütz, M.; Müller-Plathe, F. *J. Comput. Chem.*, in press.
(8) Meyer, H.; Biermann, O.; Faller, R.; Reith, D.; Müller-Plathe, F. *J. Chem. Phys.* **2000**, *113*, 6264−6275.
(9) Faller, R.; Schmitz, H.; Biermann, O.; Müller-Plathe, F. *J. Comput. Chem.* **1999**, *20*, 1009−1017.
(10) Faller, R.; Müller-Plathe, F. *ChemPhysChem* **2001**, *2*, 180−184.
(11) Faller, R.; Müller-Plathe, F. *Polymer* **2002**, *43*, 621−628.
(12) Faller, R.; Müller-Plathe, F.; Doxastakis, M.; Theodorou, D. *Macromolecules* **2001**, *34*, 1436−1448.
(13) Faller, R. Influence of Chain Stiffness on Structure and Dynamics of Polymers in the Melt. Ph.D. Thesis, MPI für Polymerforschung and Universität Mainz, 2000.
(14) Berendsen, H. J. C.; Postma, J. P. M.; van Gunsteren, W. F.; DiNola, A.; Haak, J. R. *J. Chem. Phys.* **1984**, *81*, 3684−3690.
(15) Müller-Plathe, F. *Comput. Phys. Commun.* **1993**, *78*, 77−94.
(16) Faller, R. *Phys. Chem. Chem. Phys.* **2002**, *4*, 2269−2272.
(17) Schmitz, H.; Faller, R.; Müller-Plathe, F. *J. Phys. Chem. B* **1999**, *103*, 9731−9737.
(18) Doi, M.; Edwards, S. F. *The Theory of Polymer Dynamics*; Clarendon Press: Oxford, 1986; Vol. 73 of *International Series of Monographs on Physics*.
(19) Faller, R.; Müller-Plathe, F.; Heuer, A. *Macromolecules* **2000**, *33*, 6602−6610.
(20) Allen, M. P.; Tildesley, D. J. *Computer Simulation of Liquids*; Clarendon Press: Oxford, 1987.
(21) Grest, G. S.; Kremer, K. *Phys. Rev. A* **1986**, *33*, R3628−R3631.
(22) Pütz, M.; Curro, J. G.; Grest, G. S. *J. Chem. Phys.* **2001**, *114*, 2847−2860.
(23) Davidson, N. S.; Fetters, L. J.; Funk, W. G.; Hadjichristidis, N.; Graessley, W. W. *Macromolecules* **1987**, *20*, 2614−2619.
(24) Tsunashima, Y.; Hirata, M.; Nemoto, N.; Kurata, M. *Macromolecules* **1988**, *21*, 1107−1117.
(25) Rouse, P. E. *J. Chem. Phys.* **1953**, *21*, 1272−1280.
(26) Kuhn, W. *Kolloid Z.* **1934**, *68*, 2−15.
(27) Floudas, G.; Reisinger, T. *J. Chem. Phys.* **1999**, *111*, 5201−5204.
(28) Fetters, L. J.; Lohse, D. J.; Milner, S. T.; Graessley, W. W. *Macromolecules* **1999**, *32*, 6847−6851.

(29) Kremer, K.; Grest, G. S. *J. Chem. Phys.* **1990**, *92*, 5057−5086.
(30) Pütz, M.; Kremer, K.; Grest, G. S. *Europhys. Lett.* **2000**, *49*, 735−741.
(31) Pütz, M. Dynamik von Polymerschmelzen und Quellverhalten ungeordneter Netzwerke. Ph.D. Thesis, MPI für Polymerforschung and Universität Mainz, 1999.
(32) Pearson, D. S.; Ver Strate, G.; van Meerwall, E.; Schilling, F. C. *Macromolecules* **1987**, *20*, 1133−1141.
(33) Ryckaert, J.-P.; Cicotti, G.; Berendsen, H. J. C. *J. Comput. Phys.* **1977**, *23*, 327−341.
(34) Reith, D. Neue Methoden zur Computersimulation von Polymersystemen auf verschiedenen Längenskalen und ihre Anwendung. Ph.D. Thesis, MPI für Polymerforschung and Universität Mainz, 2001.

MA025877S